Nature Methods

Resolution doubling in live, multicellular organisms via multifocal structured illumination microscopy

Andrew G York, Sapun H Parekh, Damian Dalle Nogare, Robert S Fischer, Kelsey Temprine, Marina Mione, Ajay B Chitnis, Christian A Combs & Hari Shroff

Note: Supplementary Videos 1–11 and Supplementary Software are available on the Nature Methods website.

Supplementary Figure 1, A misaligned pinhole does not degrade resolution in a confocal microscope

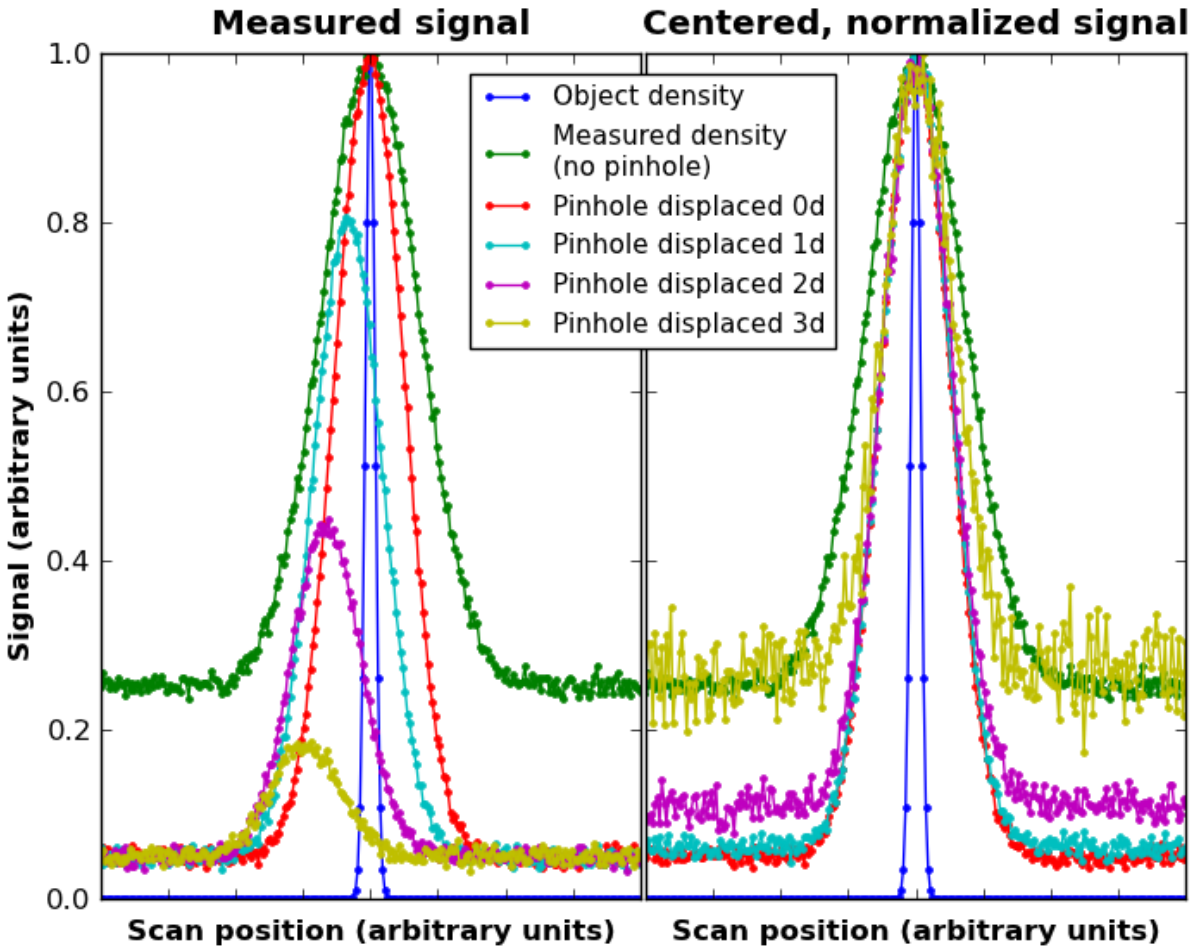

Simulation of a subdiffractive fluorescent object (blue line) imaged in 1D by a confocal microscope with different pinhole configurations. With the pinhole wide open (green line), the confocal microscope measures the microscope's excitation point spread function (PSF). A well-aligned pinhole improves resolution slightly without greatly reducing signal (red line). Displacing the pinhole transversely by one pinhole diameter (light blue line) reduces signal and shifts the peak of the signal by roughly half a pinhole diameter. Successively displacing the pinhole by one pinhole diameter at a time (purple, yellow lines) further reduces signal, and further shifts the signal peak. However, these misalignments do not cause a loss in transverse resolution. Normalized, shifted versions of the left panel plots are shown in the right panel. Apart

from different signal-to-noise levels, the measured curves with different pinhole positions have the same shape, and therefore the same resolution.

Supplementary Figure 2, The MSIM concept

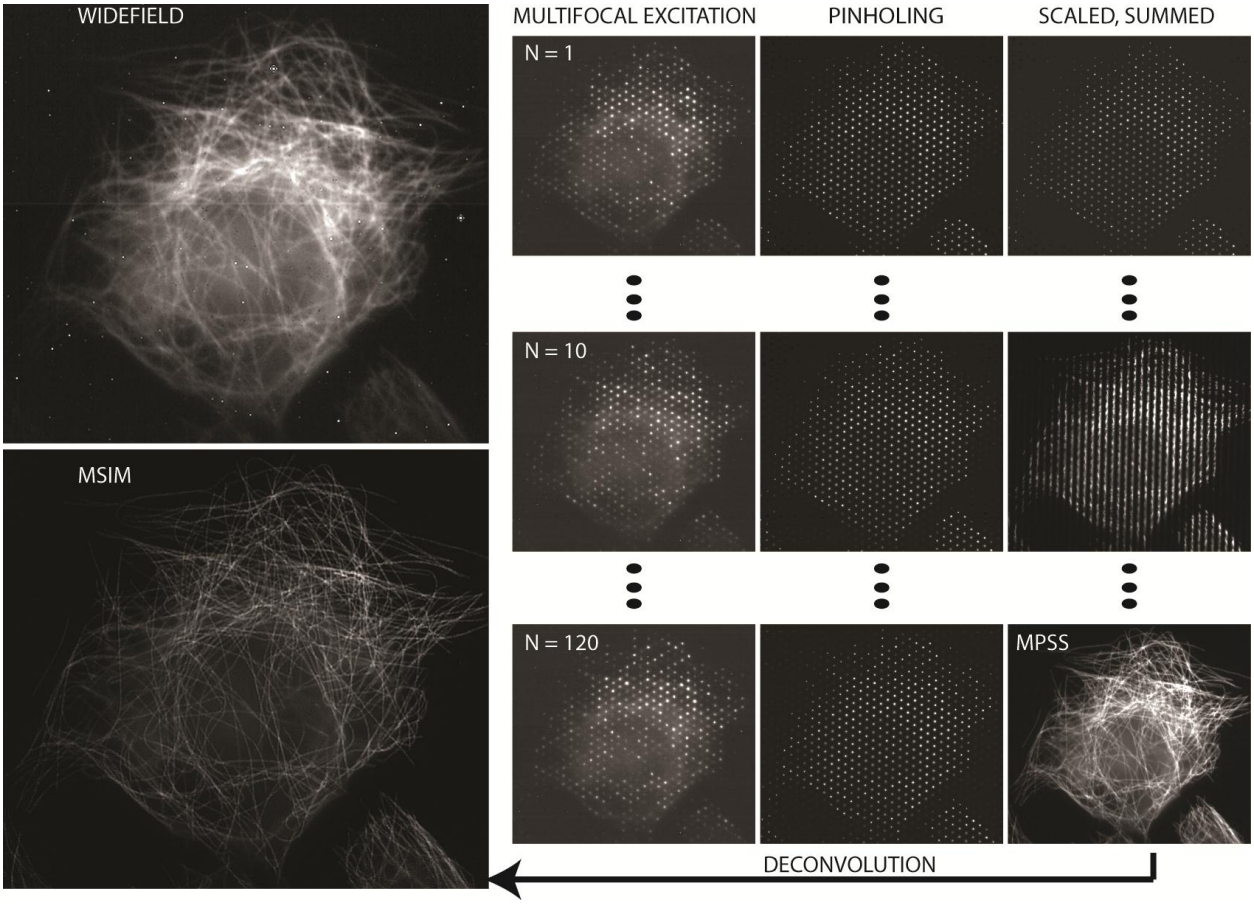

A widefield image (top left) is produced when a sample is illuminated uniformly. Alternatively, an image may be reconstructed by *(i)* exciting the sample with a sparse, multifocal excitation pattern; *(ii)* applying digital pinholes around each fluorescent focus; (*iii)* 2x scaling the resulting image; (*iv)* repeating this procedure until the sample has been fully illuminated; and *(v)* accumulating the sum of all such pinholed and scaled images. This procedure is shown (right) for the first, tenth, and final raw images of a 120 frame sequence (see also **Supplementary Video 1**). Deconvolving the summed image results in an MSIM image (lower left).

Supplementary Figure 3, Illumination system for multifocal SIM

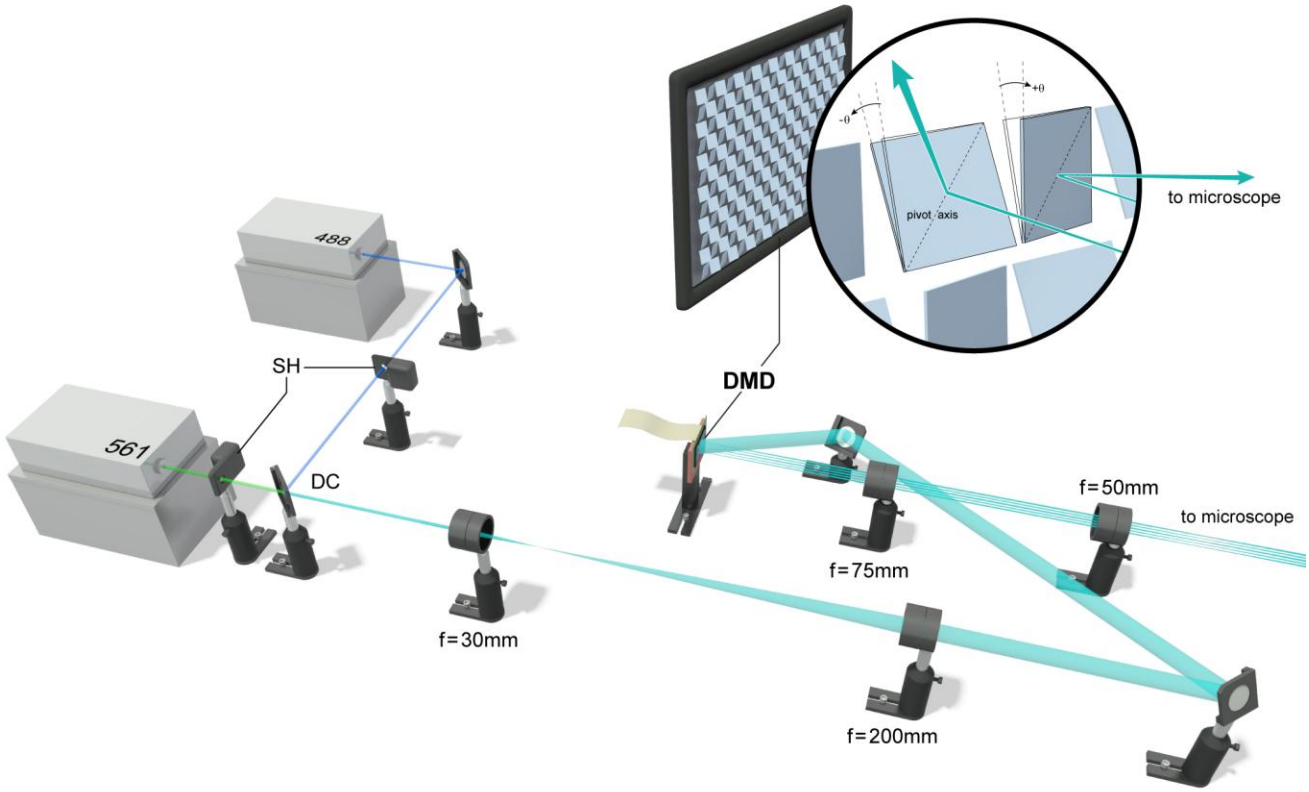

Lasers 561 and 488 are combined with a dichroic (DC), beam-expanded, and directed onto a digital micromirror device (DMD). The resulting pattern is de-expanded first by a lens pair external to the microscope (shown) and subsequently by the tube lens and 60X objective housed inside the microscope (not shown) for a total demagnification of 90X between DMD and sample. Mechanical shutters (SH) placed after each laser were used for illumination control. The number of optical elements shown is accurate, but sizes, relative distances, angles, and DMD patterns referred to in the text have been modified in order to emphasize the simplicity of the optical path.

Supplementary Figure 4, Optical sectioning as a function of excitation lattice spacing

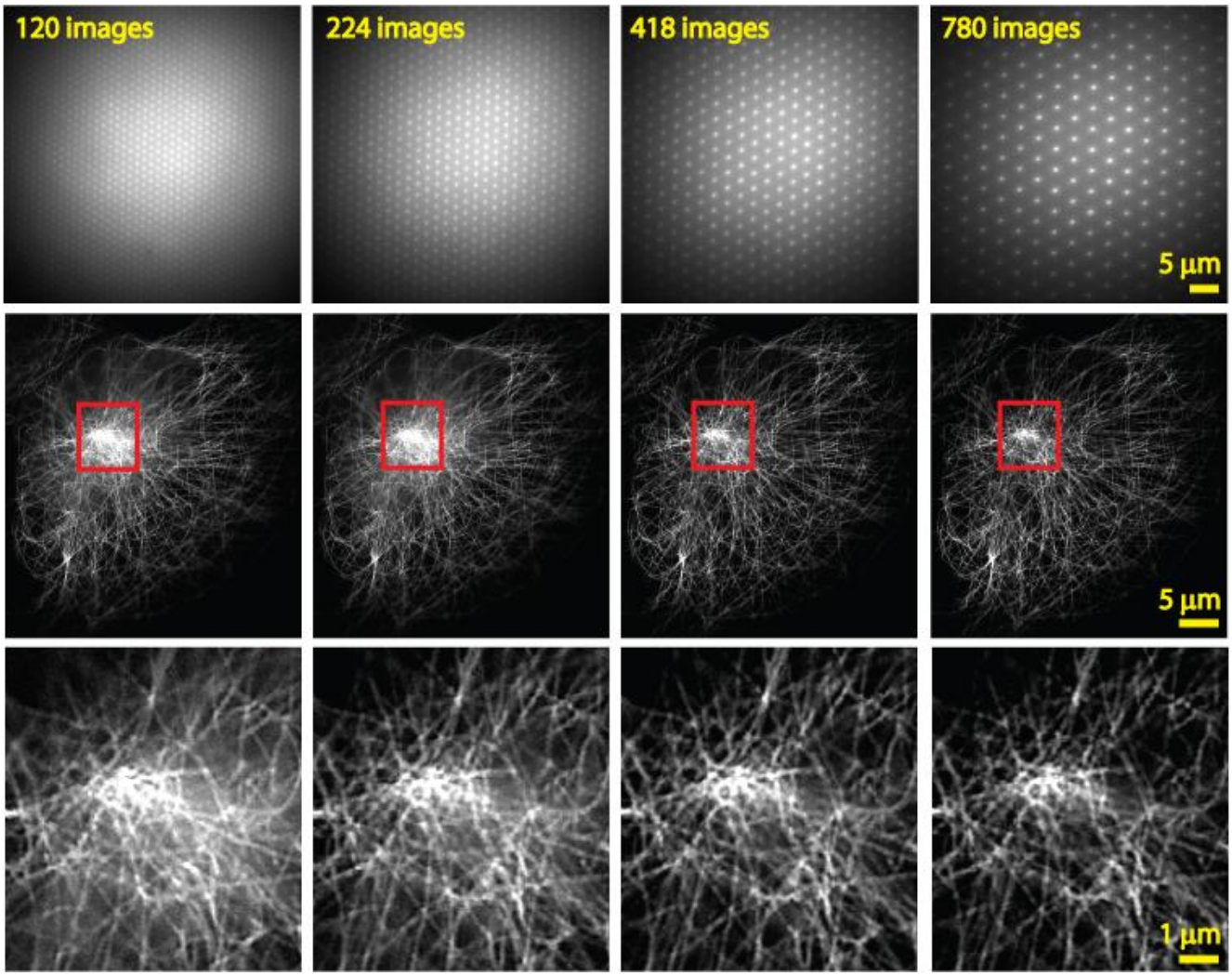

Alexa Fluor 488 labeled microtubules in a fixed cell were imaged with different spacing between excitation lattice points, in order to compare the resulting sectioning ability. Top row: single raw frames from the fluorescent solution used for calibration, also indicating the total number of images required for complete field-of-view coverage. Middle row: Reconstructed 2d slices, corresponding with lattice spacings indicated in top row. Bottom row: Higher magnification view of the red boxes in middle row. Sparser excitation lattices result in better optical sectioning, but at the cost of additional images. Images in each row share the same minimum and maximum intensities, i.e. are not 'autoscaled'.

Supplementary Figure 5, Optical sectioning as a function of digital pinhole diameter

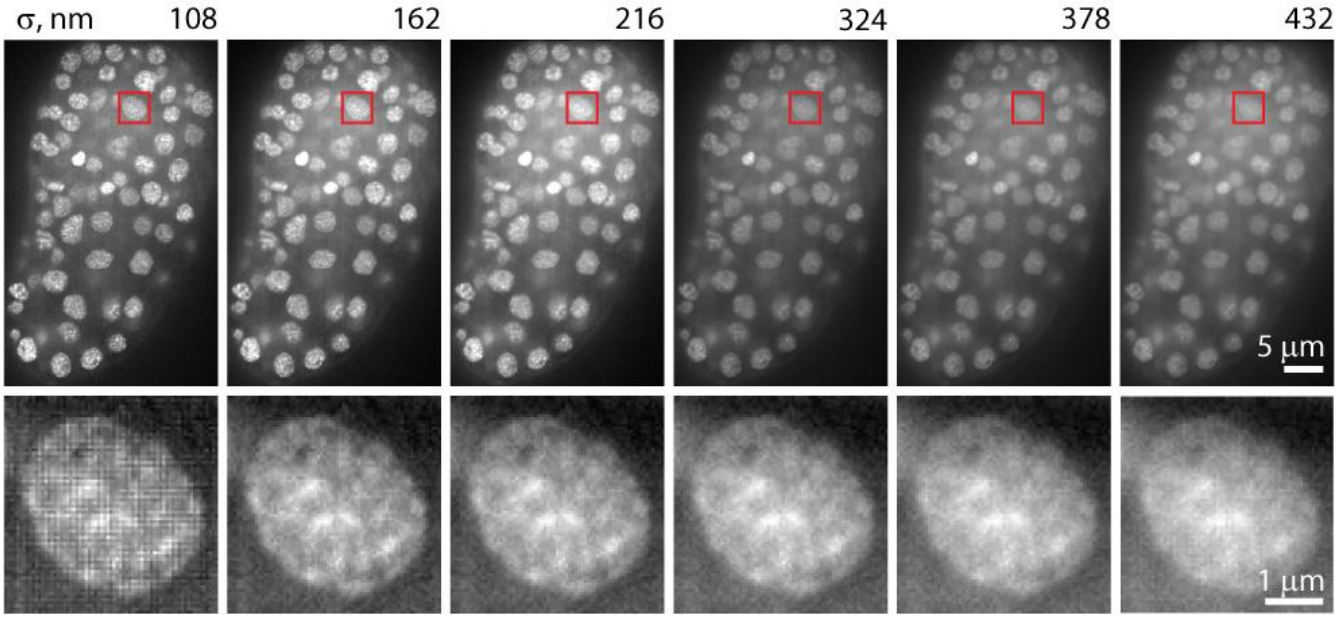

Top row: Single reconstructed 2D slices (each composed from the same 224 raw images) from a live *C. elegans* embryo, processed with different digital pinhole sizes (pinholes are Gaussian functions with standard deviation σ as indicated; 108 nm is the size of one camera pixel). Bottom row: higher magnification views of nuclei highlighted in red in top row. Smaller pinholes reject more out of focus light and increase contrast, although the very smallest pinhole size shown also introduces a slight artifact, visible as horizontal and vertical lines in the zoomed nuclei. As smaller digital pinholes pass significantly less light than larger pinholes, images are 'autoscaled' (i.e. each image has different minimum and maximum image intensities). To emphasize the effect of the digital pinholes, images were not deconvolved. For all figures in the paper, a pinhole with σ = 162 nm was used.

Supplementary Figure 6, Comparison between widefield and deconvolved images

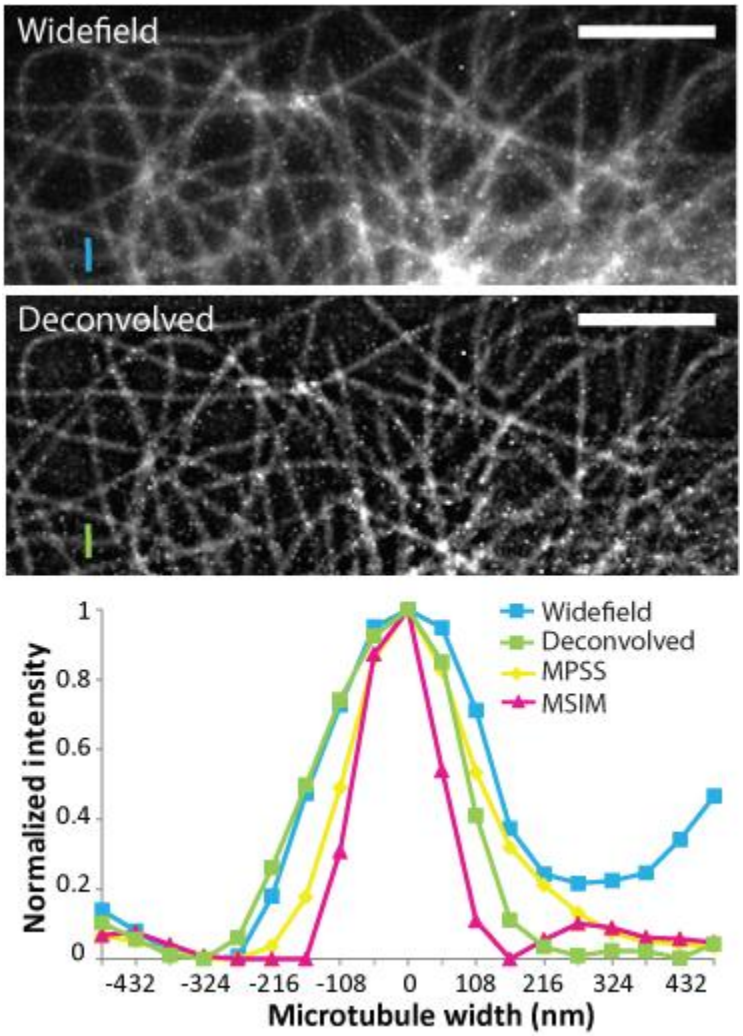

Widefield (top) and deconvolved, widefield (middle) images, with accompanying lineouts (bottom, compare to **Fig. 1d**). Scalebars: 5 μm. Deconvolved images improve contrast, with only slight improvement in lateral resolution (FWHM of highlighted microtubule: widefield 299 nm; deconvolved microtubule 254 nm, MPSS 224 nm; MSIM 145 nm). Deconvolution is not expected to improve resolution beyond the diffraction limit when applied to conventional widefield images. MPSS images, however, are expected to contain higher spatial frequencies that allow higher resolution after deconvolution[1].

Supplementary Figure 7, Apparent size of subdiffractive beads after multifocal structured illumination

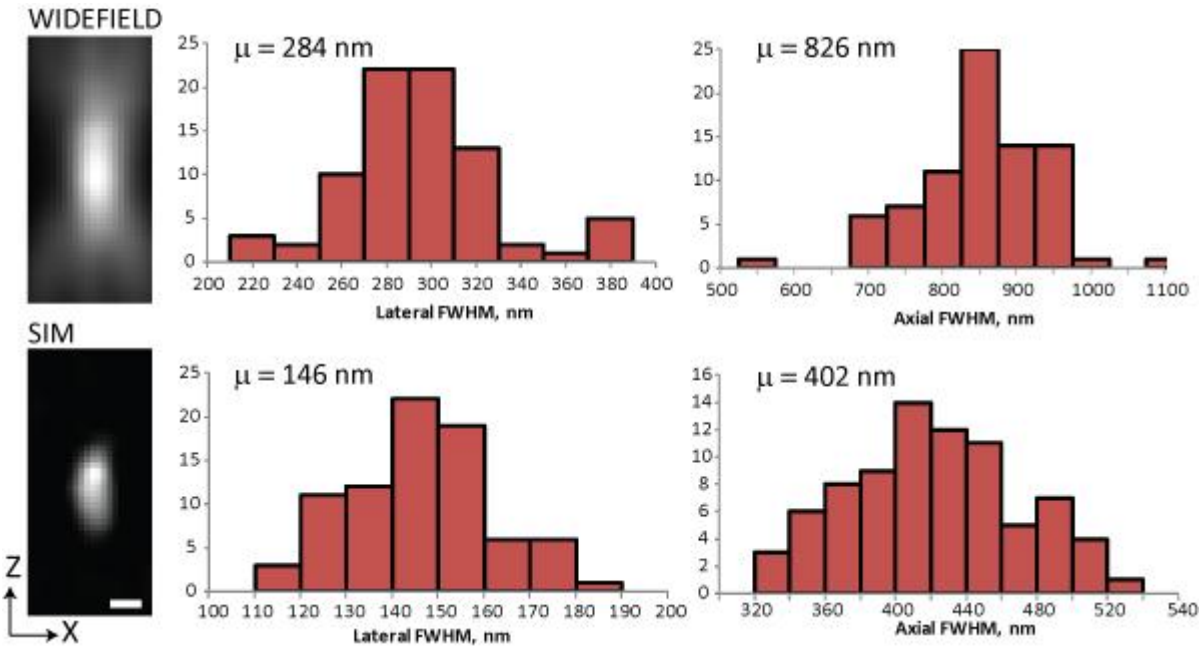

Example XZ average intensity projections (left) and histograms of apparent size (right) of 110 nm yellow-green fluorescent beads. Beads were mounted in Fluoromount G and imaged in the multifocal structured illumination microscope in either widefield (top row) or SIM (bottom row) mode. Histograms show the measured distribution of lateral and axial full width at half maximum (FWHM) values from 80 beads. Beads were identified manually and FWHM values were estimated from average XZ intensity projections after resampling the data with a slightly finer pixel size (36 nm) than shown elsewhere in the text. Mean FWHM values are also displayed above each distribution, and the scalebar shown in the average XZ projection is 200 nm. Data were acquired with a 1.45 NA, 60x TIRF objective.

Supplementary Figure 8, Subdiffractive features revealed by 3D MSIM

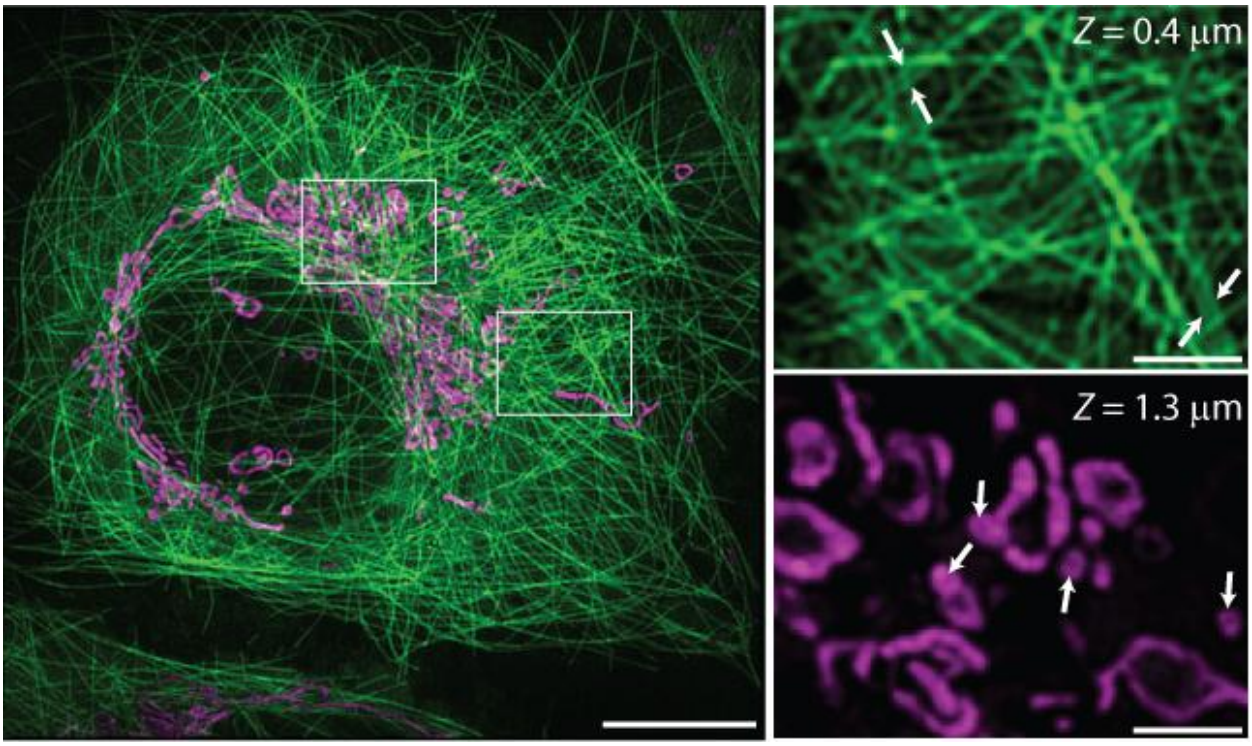

Maximum intensity projection (left) of dataset presented in **Fig. 2**, also indicating higher magnification views (right) of the white boxed regions. Top right: microtubules 0.4 μm from coverslip surface. Bottom right: mitochondria 1.3 μm from coverslip. Arrows highlight separations between paired microtubules or voids within mitochondria with subdiffractive dimensions. Left scalebar, 10 μm; right scalebars, 2 μm.

Supplementary Figure 9, Comparison between MSIM and confocal microscopy

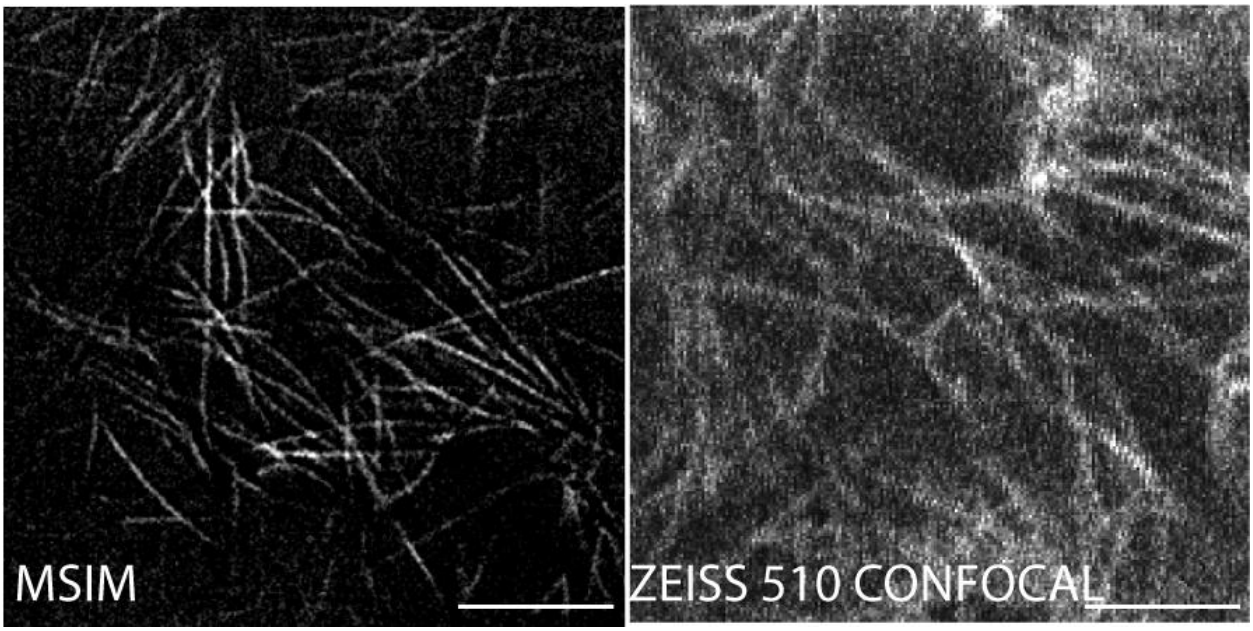

MSIM (left) and confocal (right, taken on a Zeiss 510 confocal laser scanning microscope) images taken in the epidermis of the zebrafish, ~4 μm into the stack. Scalebars, 5 μm. See also **Supplementary Video 6**.

Supplementary Figure 10, MSIM in a live nematode embryo

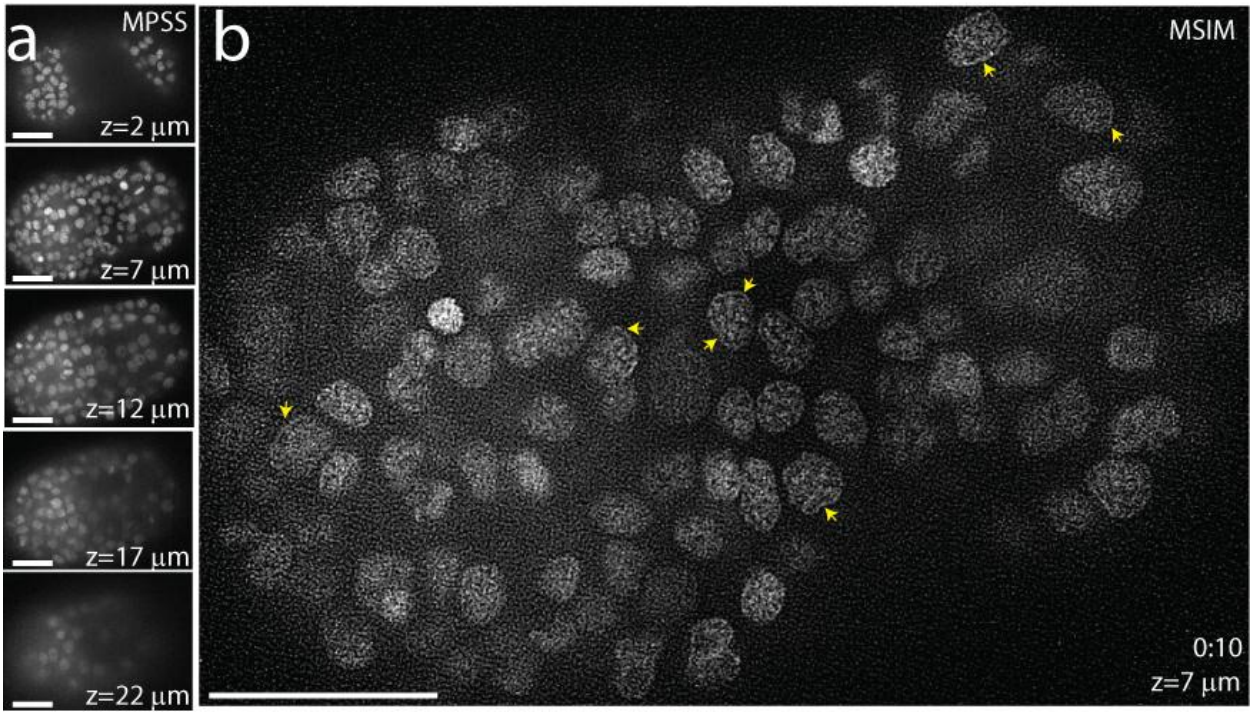

4D MSIM datasets were collected on live nematode embryos expressing GFP-histones (25 slices per volume, spaced 1 μm apart, 1 Hz 2D imaging rate, 1 volume collected every 5 minutes for a total of 35 volumes). (**a**) Selected slices at different axial depths from the first MPSS volume in the time series, demonstrating degradation in image quality as a function of depth. (**b**) MSIM image obtained by applying 2D deconvolution to the MPSS data at indicated time point and axial depth. Yellow arrows indicate fluorescent signal along nuclear periphery with apparent thickness ~ 160 nm. See also **Supplementary Video 10.** All scale bars 10 μm.

Supplementary Note 1, Equivalence of ISM procedure and operating a confocal microscope with a stopped-down pinhole

The resolution of a confocal microscope depends on the diameter of its confocal pinhole. In theory, the transverse resolution can be ~ √2-fold better than the resolution of an equivalent widefield microscope. Achieving this resolution requires the confocal pinhole to be much smaller than the magnified image of a point emitter[2]. In practice, confocal microscopes are seldom operated with such a small pinhole, because too much light is rejected, giving an unacceptable signal-to-noise ratio.

In ISM[1], the point detector in a confocal microscope is replaced with a multi-pixel detector, such as a CCD or CMOS camera, and post-processing improves the resolution √2-fold over widefield microscopy without sacrificing signal-to-noise. The mathematics behind this resolution gain is clear, but little physical interpretation is given.

We offer the following interpretation. If each pixel in the multi-pixel detector is much smaller than the image of a point emitter, one can consider each pixel in the detector to be a tightly closed confocal pinhole, with some degree of transverse misalignment. As the illumination beam sweeps through the sample, any single detection pixel collects the same image that a confocal microscope with a tightly closed, misaligned pinhole would collect.

Interestingly, transverse misalignment of the confocal pinhole does not degrade transverse resolution (**Supplementary Fig. 1**). Measured signal decreases, and the measured image shifts, but the shape of the measured feature is unaffected. Since each pixel in ISM is misaligned from the optimal confocal pinhole position by a different amount, each single-pixel image is shifted and attenuated by a different amount, but the images are otherwise identical. The processing in ISM simply shifts the high-resolution image collected by each pixel by an appropriate amount before summing the images. The resulting image retains the high resolution of a tightly-closed pinhole, but without sacrificing light.

Since a pinhole misaligned by x shifts an image by ~x/2 (**Supplementary Fig. 1**), we shift the light collected by each pixel toward the closest illumination focus by half the distance that separates the pixel from the focus. This is why we choose a scaling factor of 2 in our processing. Finally, we note that in ISM pixels are stationary relative to the illumination, but in

MSIM pixels are stationary relative to the sample, requiring a change of coordinates when applying the ISM processing.

Supplementary Note 2, Use of the DMD in data acquisition

Proper DMD operation requires understanding a few important details:

* The DMD is a two-dimensional diffraction grating, and will diffract light in many different directions. Proper shielding is crucial for eye safety.

* The output beam of the DMD is not the zero-order diffraction, so different input beam colors will diffract in many different directions. We primarily operate with only a few isolated pixels 'ON' at a time, which diminishes the importance of this effect. For 'widefield' illumination, however, this requires different input laser colors to have different input directions in order to share a common output direction.

* Because the angle of incidence does not equal the angle of diffraction, the input beam suffers some anamorphic magnification, distorting the illumination beam shape. For our application, beam shape is not crucial.

* For output normal to the DMD face, the input laser beams come in at an unusual angle, neither in a horizontal nor a vertical plane with respect to the other system optics.

* The DMD pixels have a finite contrast ratio. Even with all pixels in the 'OFF' state, some light will still reach the sample. We used mechanical shutters in each illumination beam to turn illumination truly 'OFF' during any pause in acquisition.

* The pixels at the outer perimeter of the DMD are always in a deflected state and are not user-addressable. While it would seem that two input angles may be chosen for normal output, in fact only one of these allows the DMD to be fully OFF.

Supplementary Note 3, Use of the sCMOS camera in data acquisition

The pco.edge sCMOS camera is a relatively new product, and its behavior differs from a CCD in several important ways. Optimal operation requires a thorough understanding of the camera's behavior:

* The region of interest of the camera must be vertically centered on the camera chip, constraining optical alignment. The horizontal region of interest is coarsely adjustable.

* The camera must be in 'global shutter' mode. In 'rolling shutter' mode, different rows of the camera will be exposed at different times, making synchronization between exposure and illumination impossible.

* In 'global shutter' mode, the camera's hot pixel correction does not work, which we compensated for with post-processing (see below). Post processing also compensates for the spatially non-uniform noise across the chip.

* The trigger mode must be set to 'External Exposure Start', where a trigger pulse starts the exposure, but the camera software controls exposure duration. 'External Exposure Control' does not work in global shutter mode.

* We set the camera's exposure time to 2.2 ms; any longer, and the camera does not finish exposure and readout in time to accept the next trigger pulse. Interestingly, decreasing the exposure time at this repetition rate does not affect when the exposure ends, but rather when the exposure begins. This behavior is not obvious, and is not currently documented.

* After any substantial pause, the first three frames of acquisition at this repetition rate are extremely noisy and unsuitable for precise measurement. For this reason, we append three blank frames to the start of each illumination pattern sequence, and do not record the first three camera exposures to disk. This behavior is also not obvious or documented.

* We initially planned to use the camera as the master clock for our system, but found that in 'Auto Sequence' trigger mode, the camera sends out extra trigger signals at the end of the acquisition. This would result in undesirable light dose to the sample, so we abandoned this approach, instead using the DMD as the master clock.

* We initially mounted the camera directly to the microscope base. However, the fan in the camera causes substantial vibration of the sample. Mounting the camera directly to our optical table with no mechanical contact between the camera and microscope body was essential for high-resolution measurements.

Supplementary Note 4, MPSS processing

Data processing steps are summarized as follows:

1. Automatic lattice detection

2. Pinhole masking

3. Local contraction/scaling

4. Summing

In more detail,

1. Automatic lattice detection:

In order to perform pinhole masking and local contraction, the positions of each illumination focus must be found. Five vectors completely specify the locations of all excitation foci in an MPSS image acquisition series:

a) Lattice vectors

Two lattice vectors specify the 2D displacement between any two neighboring illumination spots. Any lattice point displaced by a lattice vector will fall on another lattice point.

b) Offset vector

The offset vector specifies the absolute position of the illumination spot closest to the center of the first image in a multifocal excitation series.

c) Shift vectors

The shift vectors specify the distance each illumination spot moves between consecutive images. Since the multifocal patterns are rastered in two dimensions, there is a 'fast' shift vector applied at every step of the scan, and a 'slow' shift vector applied when the 'fast' shift vector has finished illuminating one row.

Due to thermal drift, the exact locations of the illumination spots may vary in time, so accurately extracting all vectors from each measured dataset gives the best performance. We use the following algorithm:

a) Obtaining the lattice vectors

*Apodize and Fourier transform each raw image

*Average the Fourier magnitudes

The structure of the sample distorts the apparent positions of illumination foci, so fitting apparent peak locations does not give accurate results. Consecutive images are shifted by an amount not initially known, so averaging consecutive images doesn't work either. However, the magnitude of the Fourier transform of the raw images is also a periodic lattice of peaks. Since the peak locations in Fourier space don't depend on shifts in the spatial domain, we average the Fourier magnitudes of the raw data images to get a high signal-to-noise measurement of peak locations in Fourier space. Before Fourier transformation, we multiply each raw image by a Hann window to prevent ringing in the Fourier domain.

*Bandpass filter the Fourier magnitudes

*Search for spikes in the Fourier domain

Since the illumination is a periodic lattice, we expect the raw images' summed Fourier magnitude to also be a periodic lattice of peaks. We now desire to measure the dimensions of this lattice accurately, so we start by finding local Fourier maxima, which are either lattice elements, or noise.

*For the three lowest spatial frequency spikes, look for harmonics

*Given the location of three candidate low-frequency spikes with harmonics, search for spikes at their vector sums and differences. These spikes compose the lattice in the Fourier domain.

Peaks in a periodic lattice predict the location of other peaks in the same lattice. Every lattice point in Fourier space is located at the vector sum of an integer number of Fourier lattice vectors. Local maxima due to noise, however, are unlikely to have harmonics.

*Solve the resulting system of equations by linear least squares to obtain three Fourier lattice vectors.

Any single peak in the Fourier domain will have some positional error due to noise or pixelization. The method of least squares lets us combine the information given by each peak for a more accurate measurement of the lattice dimensions. We note that any two lattice vectors determine the third.

*Sum the Fourier lattice vectors to give an error vector. Subtract one-third of this error vector from each Fourier lattice vector.

The three Fourier lattice vectors should sum to zero, but usually don't. Enforcing this constraint substantially improves the algorithm's accuracy.

*Pick any two Fourier lattice vectors and transform them to obtain real-space lattice vectors.

Obtaining the two lattice vectors for the illumination pattern makes it substantially easier to measure the offset vector and shift vectors.

b) Obtaining the offset vector

*Median filter the first raw image

Our camera suffers from several 'hot pixels', which can disrupt the following steps. A 1-pixel median filter eliminates these hot pixels with only mild image distortion.

*Construct a lattice of points from the measured lattice vectors, with an offset vector of zero

*From the median-filtered raw image, extract a set of smaller images centered at each lattice point, using interpolation for subpixel centration

*Average these smaller images to form a 'lattice average' image

Unless the sample is a uniform fluorescent object, any single glowing spot in the first raw image is unlikely to be centered on an illumination spot. However, unless the sample is highly periodic, the displacement of any single glowing spot from the nearest illumination spot is likely to be random. By averaging the images centered on each lattice point, these random displacements will cancel, leaving a set of intensity peaks centered on the illumination spots.

*Find the brightest pixel in the lattice average.

*Use interpolation to estimate the subpixel position of the peak intensity in the lattice average.

The offset of this peak from the center of the lattice average is the offset vector.

c) Obtaining the shift vectors

*Construct the set of expected Fourier peak locations from the measured Fourier lattice vectors

*For each Fourier peak location, extract its phase versus image number from the transformed raw data

*Phase-unwrap each series to remove 2π jumps

The magnitude of the Fourier transform of each raw image is independent of shifts of the raw images. Information about shifting is encoded in the phase of the Fourier transforms. As we already computed these Fourier transforms to obtain the lattice vectors, this step is relatively fast.

*Reshape each phase series to a 2D array with the same dimensions as the scan pattern (e.g., 16 pixels x 14 pixels)

*Fit a line to the average slope of each phase series in both the 'fast' and 'slow' directions

In each consecutive raw image, the illumination shifts by $\boldsymbol{X_{FAST}}$. At the end of each row, the illumination also shifts by $\boldsymbol{X_{SLOW}}$. If an image shifts by $\boldsymbol{X}$, the phase of a peak in Fourier space located at $\boldsymbol{k}$ shifts by $\boldsymbol{k * X}$.

*Solve the resulting system of equations for $\boldsymbol{X_{FAST}}$ and $\boldsymbol{X_{SLOW}}$.

We use least squares to combine redundant, noisy measurements to form a more accurate estimate of our shift vectors.

*Construct the offset vector for the first and last frames of the series (as outlined above in b)

*Construct the predicted offset vector in the last frame based on the current estimate of $\boldsymbol{X_{FAST}}$ and $\boldsymbol{X_{SLOW}}$

*The difference between these two vectors is an error vector. Divide the error vector by the number of slow steps taken in the scan, and subtract it from $\boldsymbol{X_{SLOW}}$

Our estimated shift vectors let us predict where we expect to find the lattice in the final frame. However, a small error in our estimate will accumulate to a larger error by the final frame. Computing the offset vector for the last frame (using the same process we did to compute the offset vector of the first frame) gives a strong constraint which greatly increases the accuracy of our estimate. Note that estimating the shift vectors must be done before applying the constraint, else we wouldn't know which two spots correspond to each other.

2. Pinhole masking:

*For each raw image, construct the set of expected illumination locations based on the vectors found above

*Use interpolation to extract a smaller subimage centered at each illumination location

*Multiply each centered subimage by a 2D Gaussian mask

This process simulates the effect of pinholes. We typically use a Gaussian with σ of 1.5 camera pixels (162 nm).

*Optional: Subtract background and multiply the centered subimage by a correction factor given by calibration data

*Optional: median filter individual hot pixels

We find it useful to measure the intensity of each illumination spot in a uniform fluorescent solution, and scale each subimage by the intensity of the illumination it receives after subtracting a background image. This has the effect of 'flat-fielding' our data, as if our highly nonuniform illumination was actually uniform. This also greatly diminishes the effect of hot pixels on the final image. Our camera had two particularly hot pixels that would still disrupt the final image, so we set them individually to the median of their neighbors.

3. Local contraction/scaling:

*Resample each masked subimage to shrink it by a factor of two

*Add each scaled, masked subimage to the processed raw image.

This step is the essence of ISM[1], i.e. it provides the √2 resolution enhancement of a confocal microscope without sacrificing signal. Since we're rescaling with interpolation, the final image pixel size can be arbitrary. We use 54 nm pixels for our processed images.

4. Summing:

*Sum the processed raw images to form a final image.

*Optional: Sum the raw images to produce a calculated 'widefield' image.

This MPSS image should have √2 better resolution than a widefield image. We also expect the processed image to show greatly improved sectioning, similar to a spinning-disk or swept-field confocal microscope. The calculated widefield image contains more read noise than a measured widefield image, so we prefer to compare MPSS images directly to measured widefield images at the same total illumination dose as an MPSS image series.

MPSS processing a single image takes 30-50 s on a 12-core workstation. In practice, we find that lattice vectors are very stable, and only the offset vector and shift vectors need to be recomputed from each raw dataset. For particularly sparse samples, automatic lattice detection

may fail. In this event, we use vectors from our calibration (fluorescent solution) dataset, and try to obtain data fast, before thermal effects cause lattice parameters to shift.

For more detail on processing, refer to the open-source code, available at code.google.com/p/msim

1 Muller, C. B. & Enderlein, J. Image Scanning Microscopy. *Physical Review Letters* **104**, 198101 (2010).

2 Pawley, J. B. (Springer Science, New York, 2006).